

Supplement of Atmos. Chem. Phys., 17, 8887–8901, 2017
<https://doi.org/10.5194/acp-17-8887-2017-supplement>
© Author(s) 2017. This work is distributed under
the Creative Commons Attribution 3.0 License.



Supplement of

Modeling the role of highly oxidized multifunctional organic molecules for the growth of new particles over the boreal forest region

Emilie Öström et al.

Correspondence to: Emilie Öström (emilie.ostrom@nuclear.lu.se)

The copyright of individual parts of the supplement might differ from the CC BY 3.0 License.

Table S1. Gas-phase precursors

Gas-phase precursor	Emission database/Emission model
α -pinene	LPJ-GUESS
β -pinene	LPJ-GUESS
Limonene	LPJ-GUESS
Other monoterpenes (treated as carene)	LPJ-GUESS
Isoprene	LPJ-GUESS
Ethane	EMEP
Butane	EMEP
Etene	EMEP
Propene	EMEP
Oxylene	EMEP
Formaldehyde	EMEP
Acetaldehyde	EMEP
MEK (Methyl Ethyl Ketone)	EMEP
Glyoxal	EMEP
Methylglyoxal	EMEP
1-petene	EMEP
2-methylpropene	EMEP
Dodecane	EMEP
Benzene	EMEP
Decane	EMEP
Ethylbenzene	EMEP
Nonane	EMEP
p-xylene	EMEP
Toluene	EMEP
Undecane	EMEP
m-xylene	EMEP
1-butene	EMEP
1,2,4-trimethylbenzene	EMEP
1,3,5-trimethylbenzene	EMEP
1,2,3-trimethylbenzene	EMEP

Table S2. Plant functional types applied in LPJ-GUESS for the simulation of BVOC emissions, and their BVOC characteristics. Emission capacities for isoprene and total monoterpenes are described in Schurgers et al. (2009b), references for the separation into α -pinene, β -pinene and limonene are provided below.

PFT	emission capacity ($\mu\text{g g}^{-1} \text{dw h}^{-1}$)					fraction of monoterpenes stored	references for speciation
	isoprene	α -pinene	β -pinene	limonene	other monoterpenes		
<i>Betula pendula</i>	0.2	0.9	0.6	0.6	3.9	0	(Hakola et al., 1998, 2001; König et al., 1995)
<i>Betula pubescens</i>	0	0.05	0.05	0	0.9	0	(Hakola et al., 2001)
<i>Carpinus betulus</i>	0	0.004	0.008	0.016	0.052	0	(König et al., 1995)
<i>Corylus avellana</i>	0	0	0	0	0	0	
<i>Fagus sylvatica</i>	0	0.5	2.0	1.0	6.5	0	(König et al., 1995)
<i>Fraxinus excelsior</i>	0	0	0	0	0	0	
<i>Picea abies</i>	0.5	2.1	1.2	0.9	1.8	0.5	(Janson et al., 1999)
<i>Pinus sylvestris</i>	0	1.8	0.2	0.2	1.8	0.5	(Janson and de Serves, 2001)
<i>Populus tremula</i>	20.0	0.6	0.2	0.8	2.4	0	(Hakola et al., 1998)
<i>Quercus robur</i>	40.0	0	0	0	0	0	
<i>Tilia cordata</i>	0	0	0	0	0	0	
Boreal evergreen shrubs	2.0	0.8	0.6	0.8	1.8	0.5	(Hansen et al., 1997)
C ₃ herbaceous	0.	0.25	0.20	0.15	0.40	0.5	(König et al., 1995)

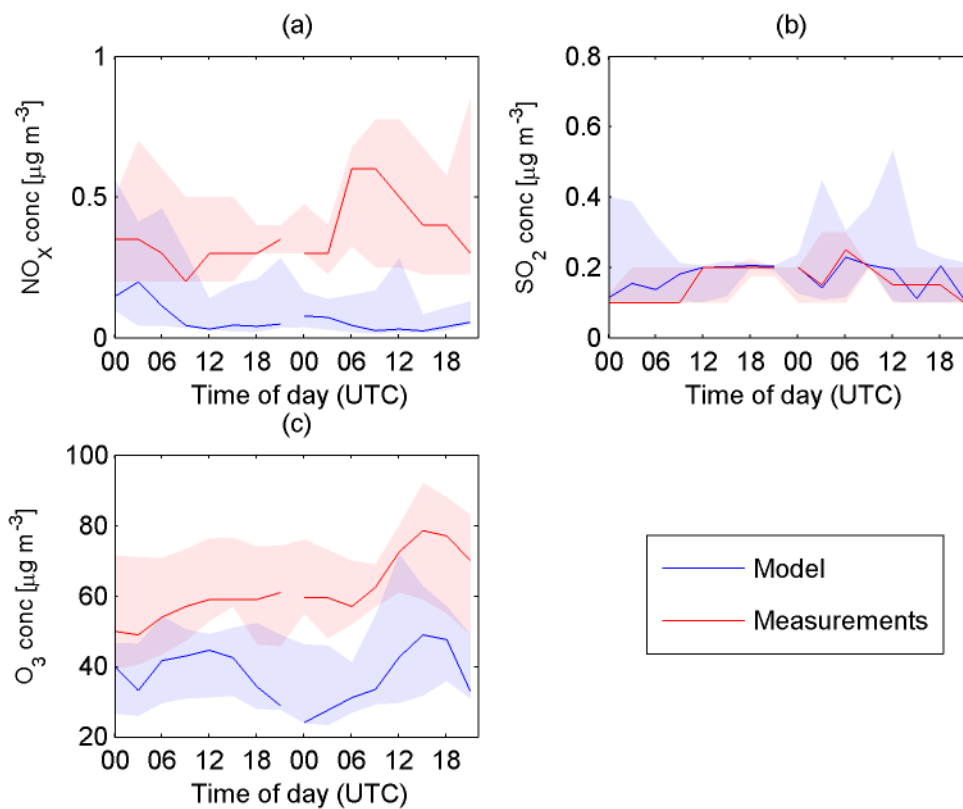


Figure S1. Median gas-phase concentration of (a) NO_x , (b) SO_2 and (c) O_3 during all chosen NPF-events at Pallas (from midnight at the day of the event to the evening the day after the start of the event) together with the 25 and 75 percentiles (shaded areas). The blue lines are the modeled results from the base-case simulation and the pink lines are the measured gas-phase concentrations.

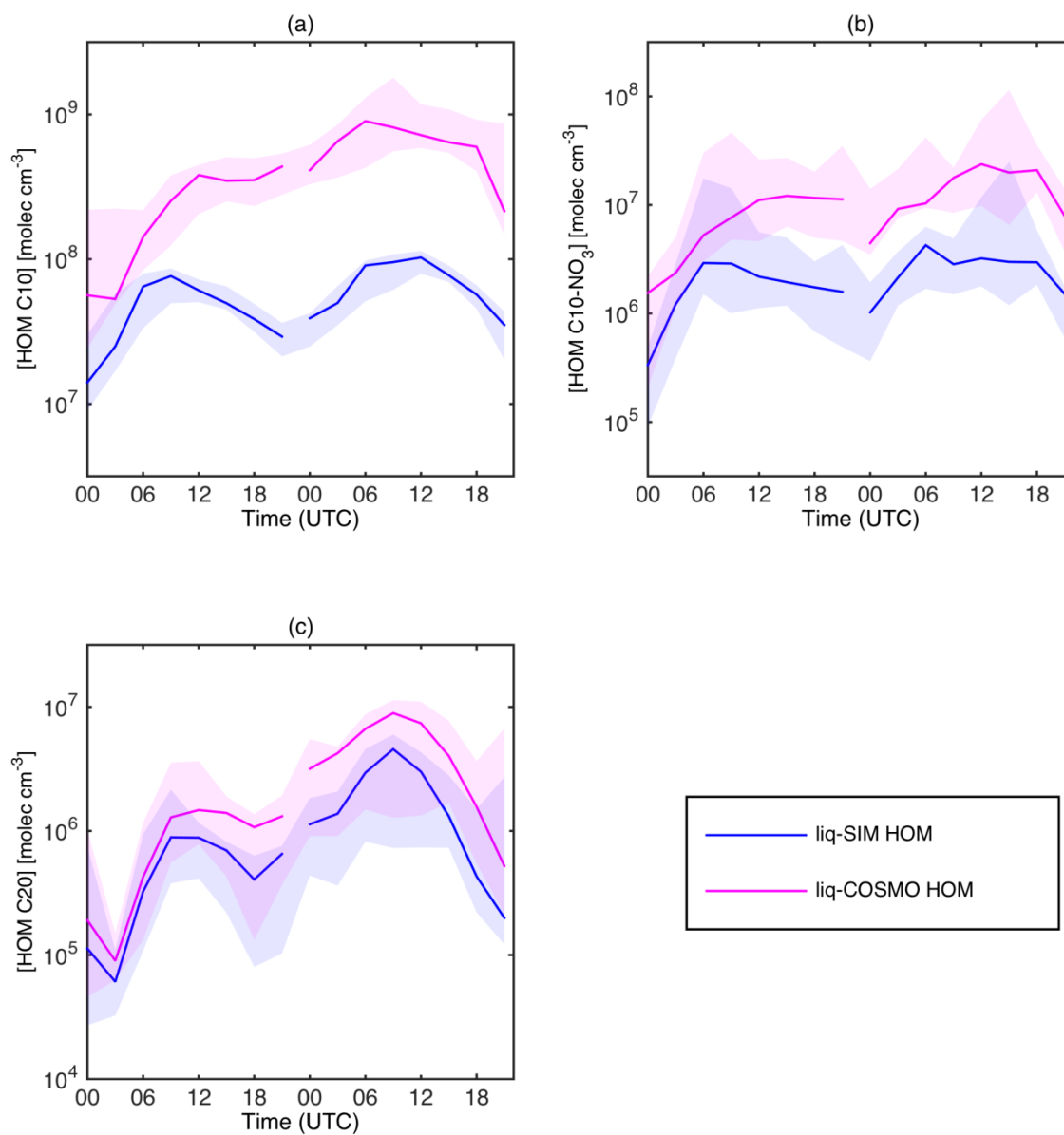


Figure S2. Median gas-phase concentration of HOMs of all chosen NPF-events at Pallas (from midnight at the day of the event to the evening the day after the start of the event) together with the 25 and 75 percentiles (shaded areas). The blue lines are the modeled results from the base-case simulation where the vapor pressures of the HOMs are estimated with SIMPOL. In the liq-COSMO HOM simulation (pink lines) the SIMPOL vapor pressures are corrected for using COSMORS (see table 1).

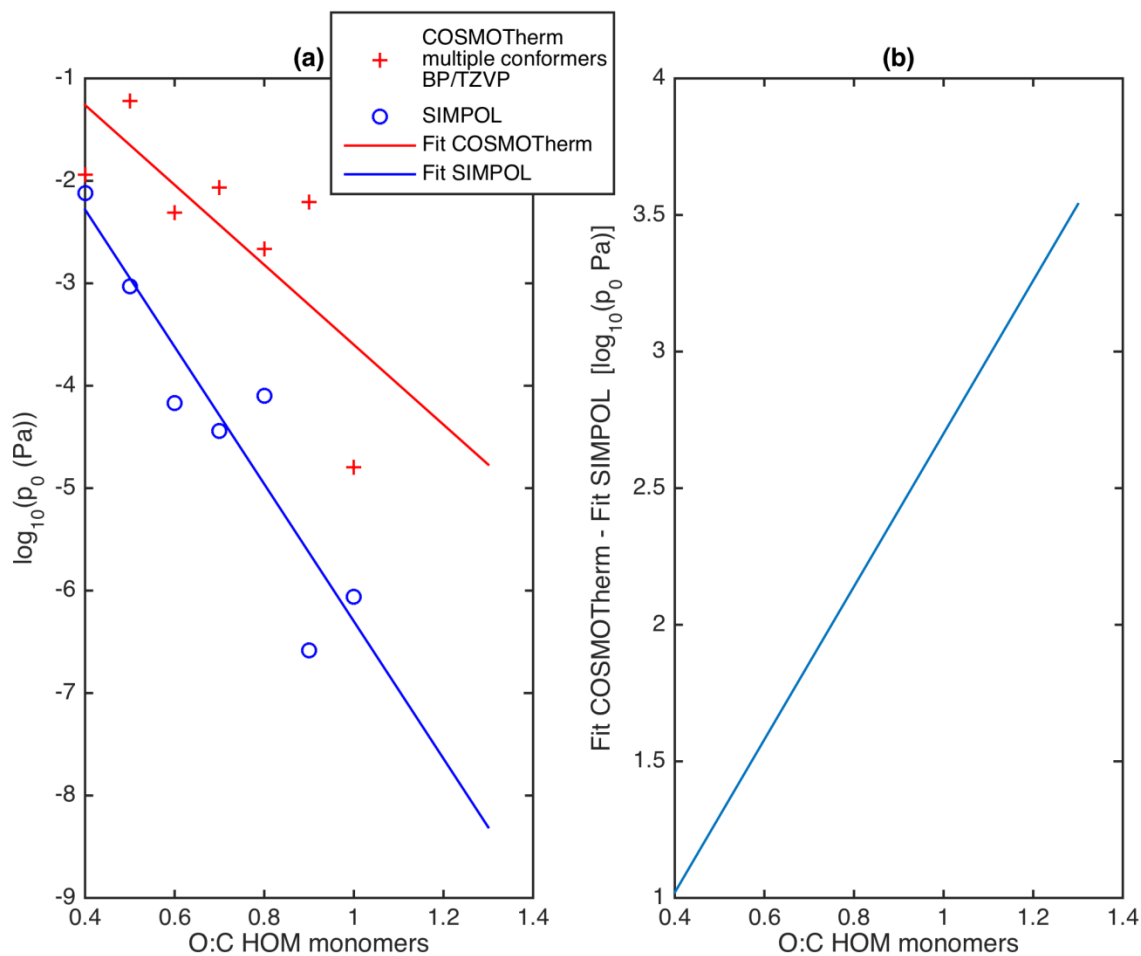
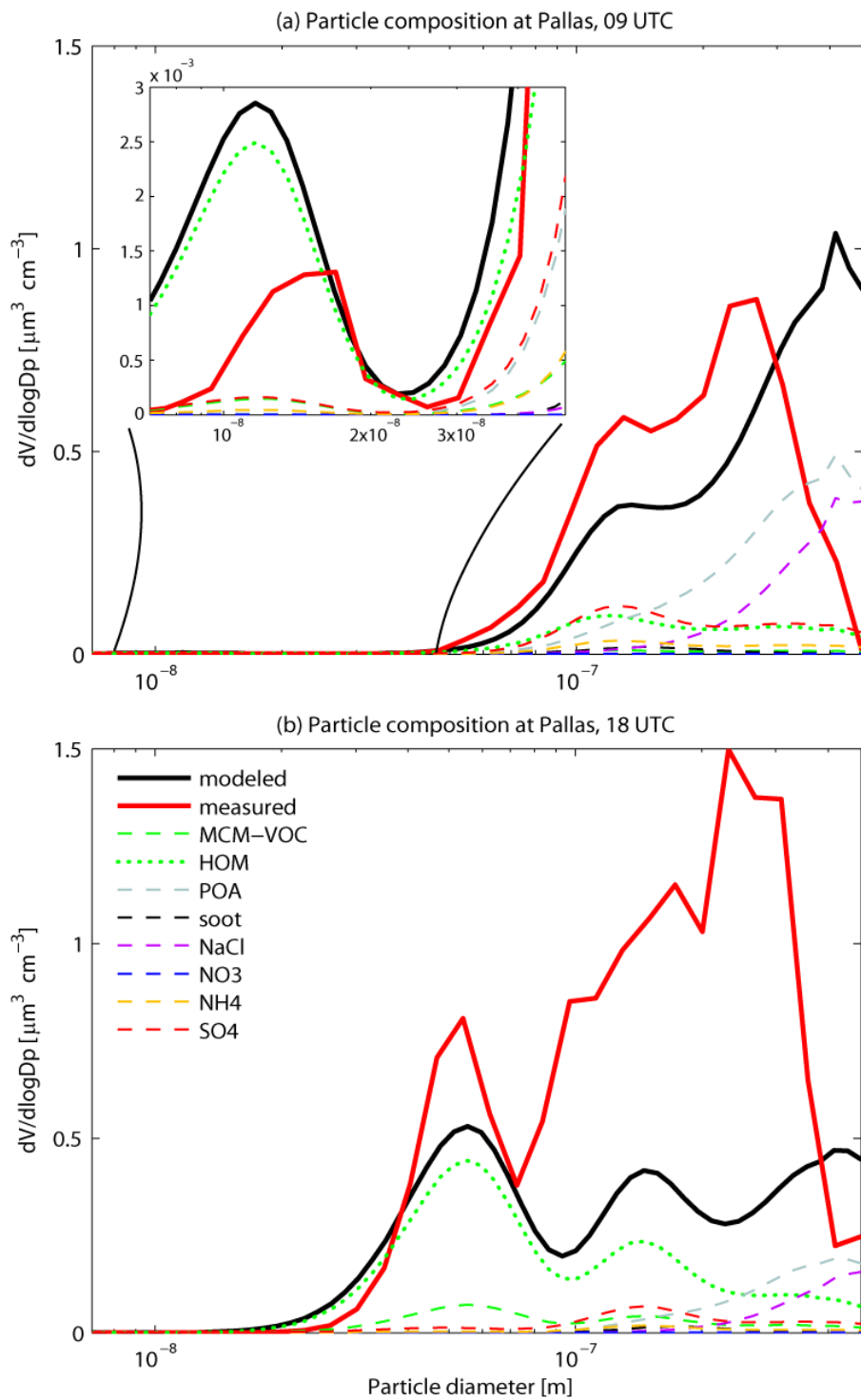


Figure S3. (a) Linear least-square fit to the pure liquid vapor pressure data points of different HOM monomers, divided into different O:C groups (O:C 0.4 – 1.0). The pure liquid vapor pressures are from Kurtén et al. (2016). The difference between the linear fits in (Fig. a) provides a correction factor (Fig. b) which was applied to the HOM pure liquid vapor pressures calculated with SIMPOL: $\log_{10}(p_0) = \log_{10}(p_{0,\text{SIMPOL}} \cdot (2.8 \cdot \text{O:C} - 0.1))$.



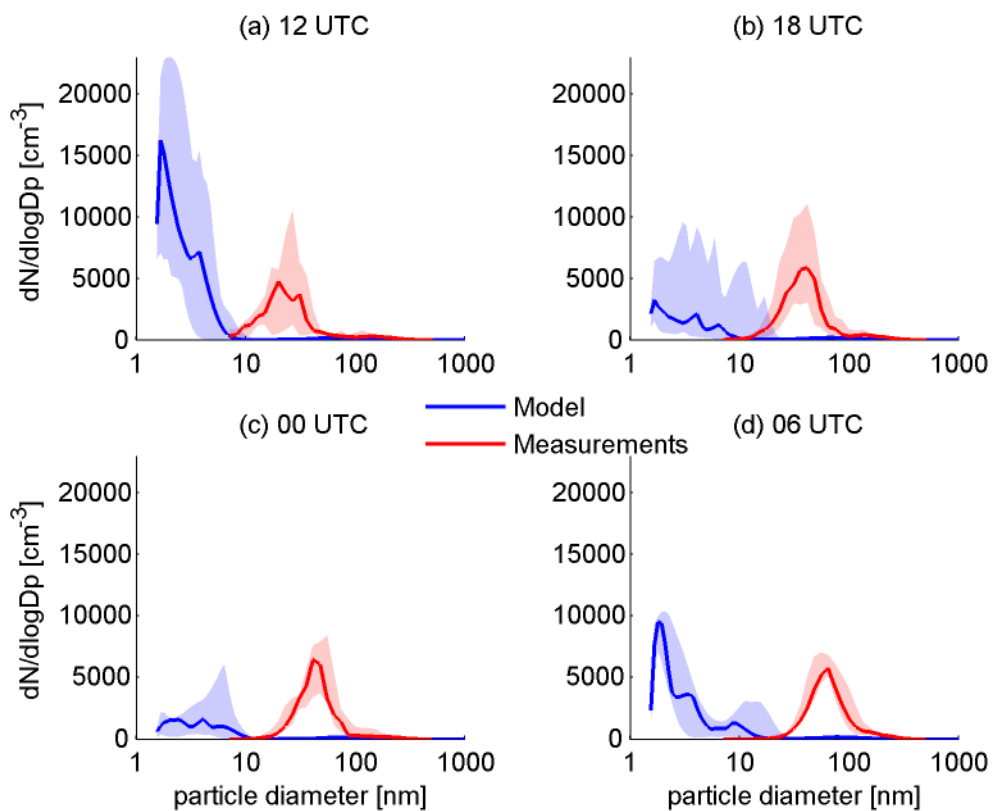


Figure S5. The modeled particles are assumed to be liquid and the formation of HOMs is excluded. Measured (red lines) and modeled (blue lines) median number size distributions at (a) 12 and (b) 18 UTC the day of the new particle formation event and (c) 00 and (d) 06 UTC the following day. The shaded areas are the values that fall between the 25th and 75th percentiles.

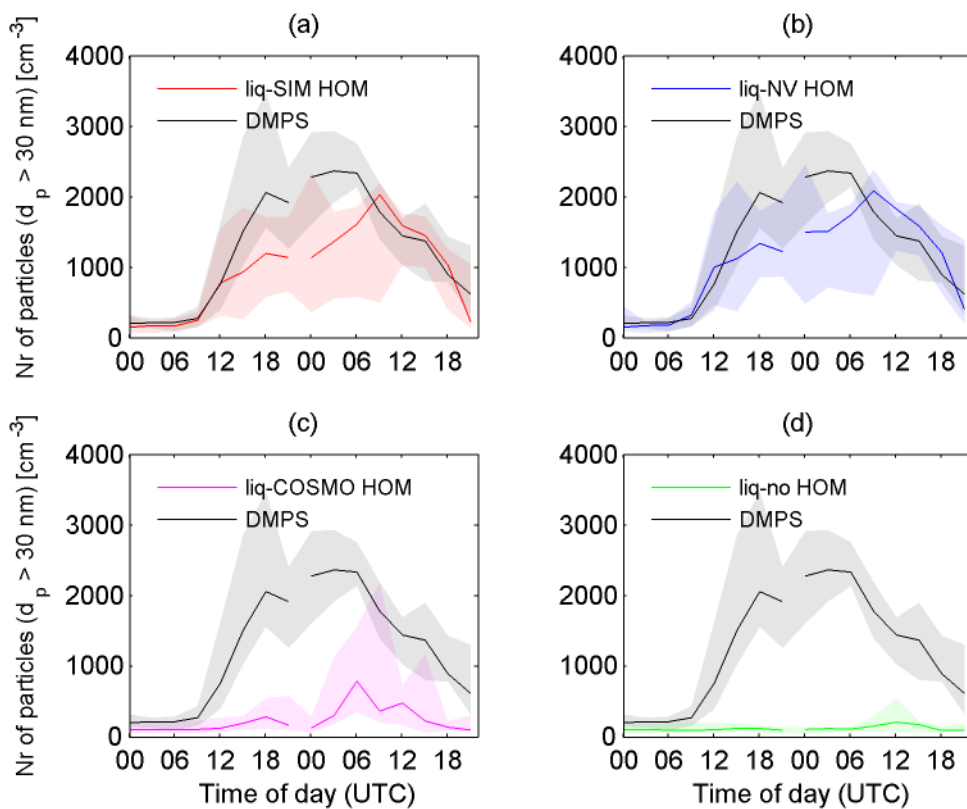


Figure S6. Median number of particles above 30 nm of all chosen NPF-events at Pallas (from midnight at the day of the event to the evening the day after the start of the event) together with the 25 and 75 percentiles (shaded areas). The black lines are the median DMPS-data from Pallas. The colored lines in (a)-(c) are the modeled median number of particles above 30 nm, using different methods to estimate the vapor pressures of the HOMs (see table 1). In (d), HOMs are excluded.

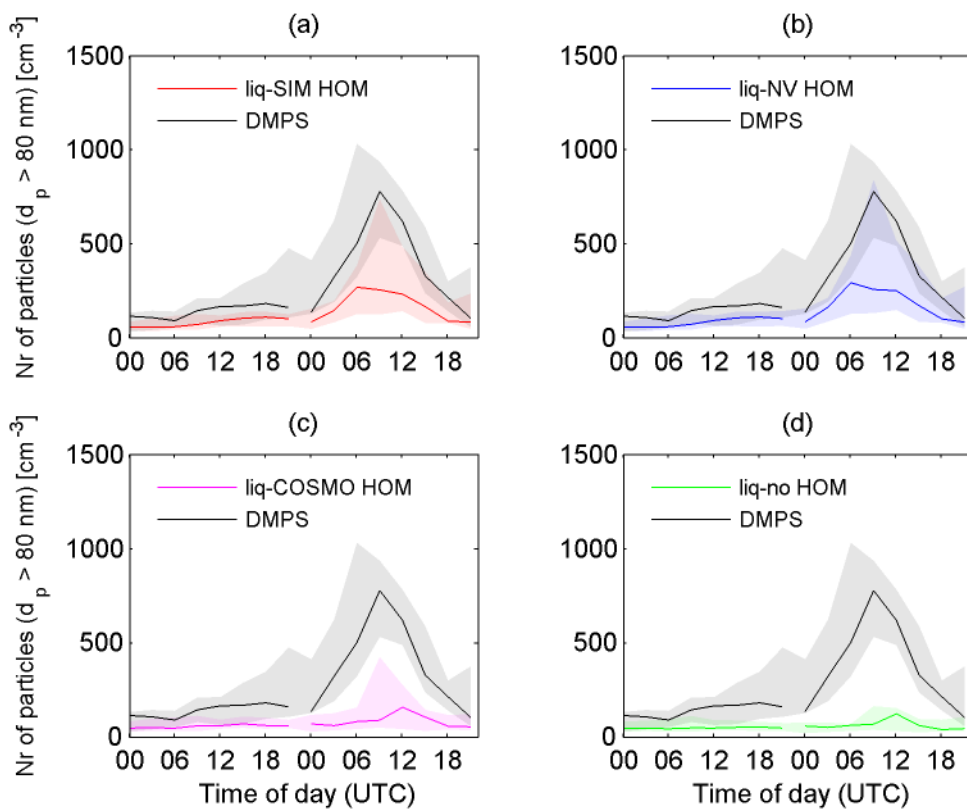


Figure S7. Median number of particles above 80 nm of all chosen NPF-events at Pallas (from midnight at the day of the event to the evening the day after the start of the event) together with the 25 and 75 percentiles (shaded areas). The black lines are the median DMPS-data from Pallas. The colored lines in (a)-(c) are the modeled median number of particles above 80 nm, using different methods to estimate the vapor pressures of the HOMs (see table 1). In (d), HOMs are excluded.

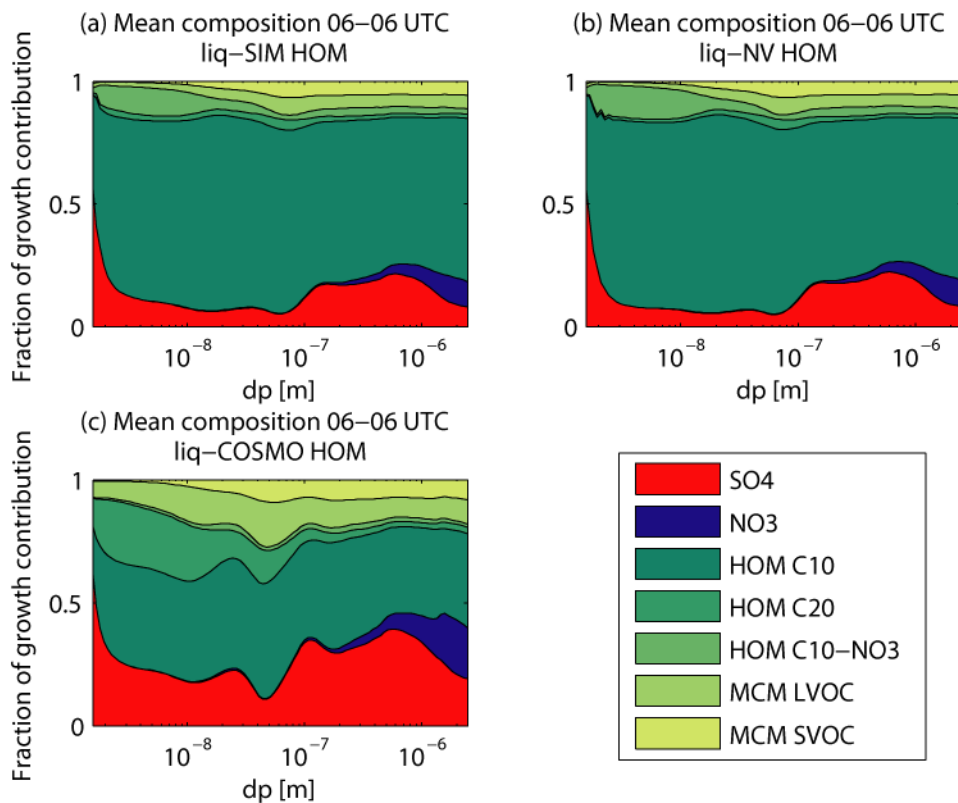


Figure S8. Mean mass fractions of each compound type that contributes to the growth of the particles during all chosen new particle formation events (from 06 UTC the morning of the event to 06 UTC the following day). In (a) the particles are assumed to be liquid with vapor pressures of HOMs estimated with SIMPOL. In (b) the particles are assumed to be liquid and the vapor pressures of HOM non-volatile. In (c) the particles are assumed to be liquid with vapor pressures of HOMs estimated with SIMPOL but corrected for with COSMO-RS. HOM C10 denote HOM monomers with 10 carbon atoms, HOM C20 is HOM dimers containing 20 carbon atoms and HOM C10-NO₃ is HOM monomers containing nitrate functional groups.

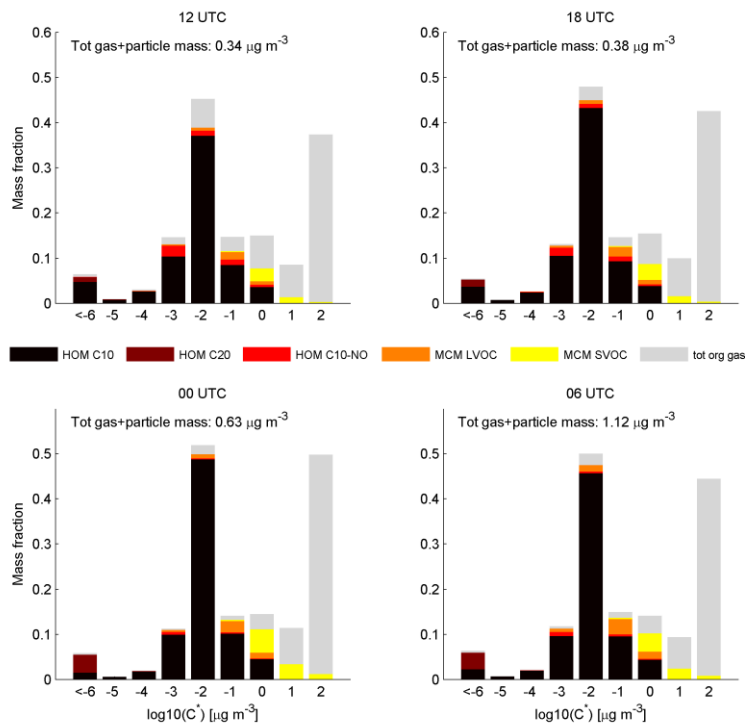


Figure S9. Modeled mean volatility distribution of SOA-components at Pallas for different times ((a) 12 UTC, (b) 18 UTC, (c) 00 UTC and (d) 06 UTC) during new particle formation events. The gray bars are the sum of all oxidized organic compounds in the gas phase with $C^* \leq 10^2 \mu\text{g m}^{-3}$. The mass in each volatility bin is normalized to the total mass (gas and particle phase) of compounds with $C^* \leq 1 \mu\text{g m}^{-3}$. The particles are assumed to be liquid and the vapor pressures of the HOMs are estimated with SIMPOL.

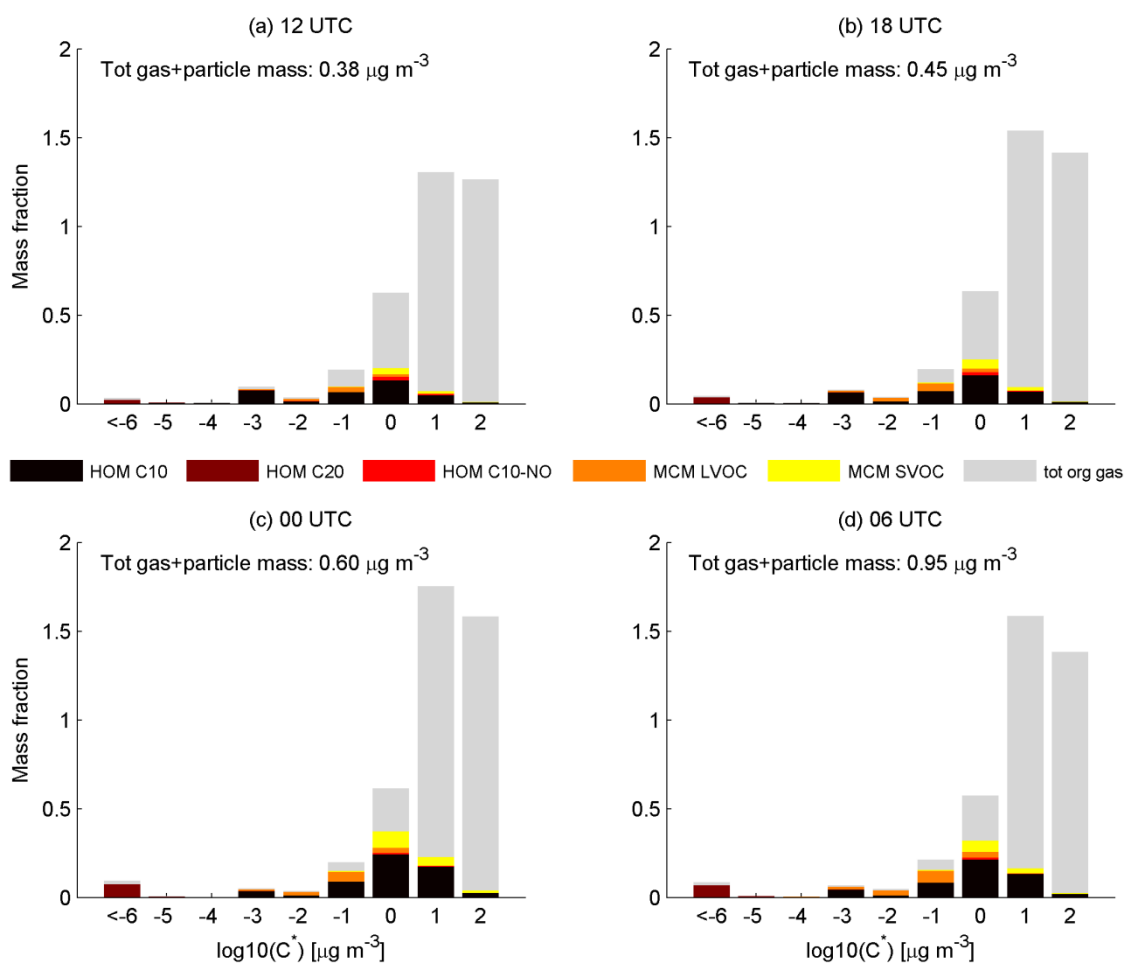


Figure S10. Modeled mean volatility distribution of SOA-components at Pallas for different times ((a) 12 UTC, (b) 18 UTC, (c) 00 UTC and (d) 06 UTC) during new particle formation events. The gray bars are the sum of all oxidized organic compounds in the gas phase with $C^* \leq 10^2 \mu\text{g m}^{-3}$. The mass in each volatility bin is normalized to the total mass (gas and particle phase) of compounds with $C^* \leq 1 \mu\text{g m}^{-3}$. The particles are assumed to be liquid and the vapor pressures of the HOMs are estimated with COSMO-RS.

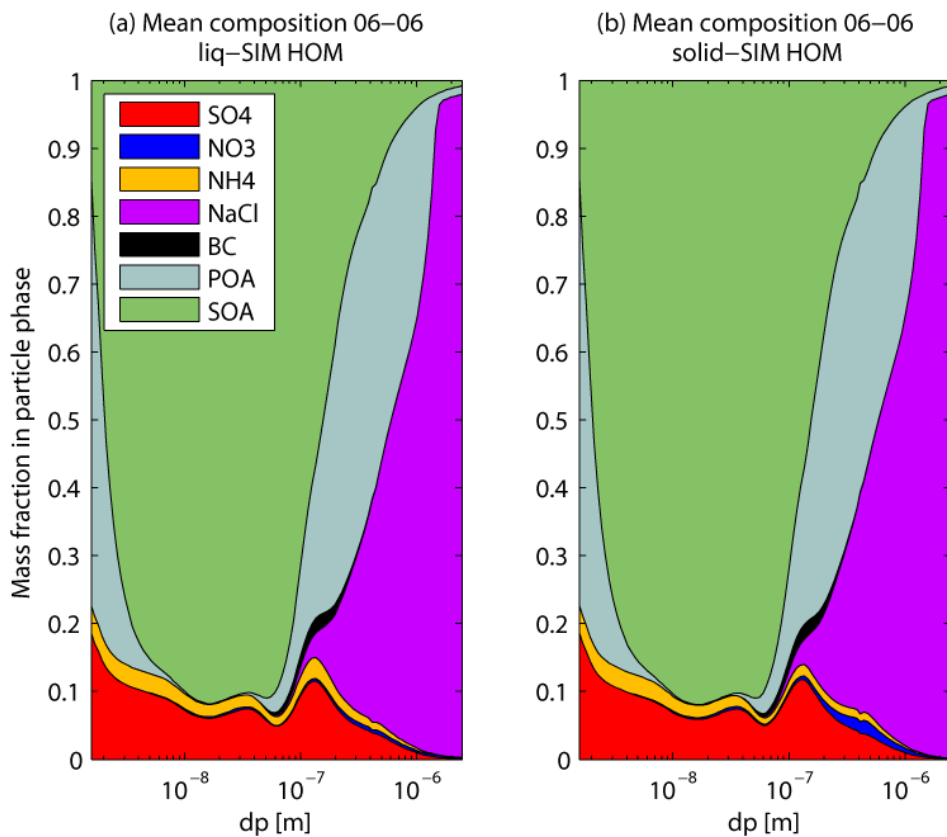


Figure S11. Mean mass fraction of each compound of the particles during all chosen new particle formation events (from 06 UTC the morning of the event to 06 UTC the following day). In (a) the particles are assumed to be liquid with vapor pressures of HOMs estimated with SIMPOL. In (b) the particles are assumed to be solid with the same vapor pressure estimation. The rather high fraction of POA (primary organic aerosols) at the smallest sizes is only subscribed as POA in the model and is actually the mole fraction of organics in the newly formed particles (assumed to be 50 %). The larger particles are background particles from the marine environment upwind Pallas.

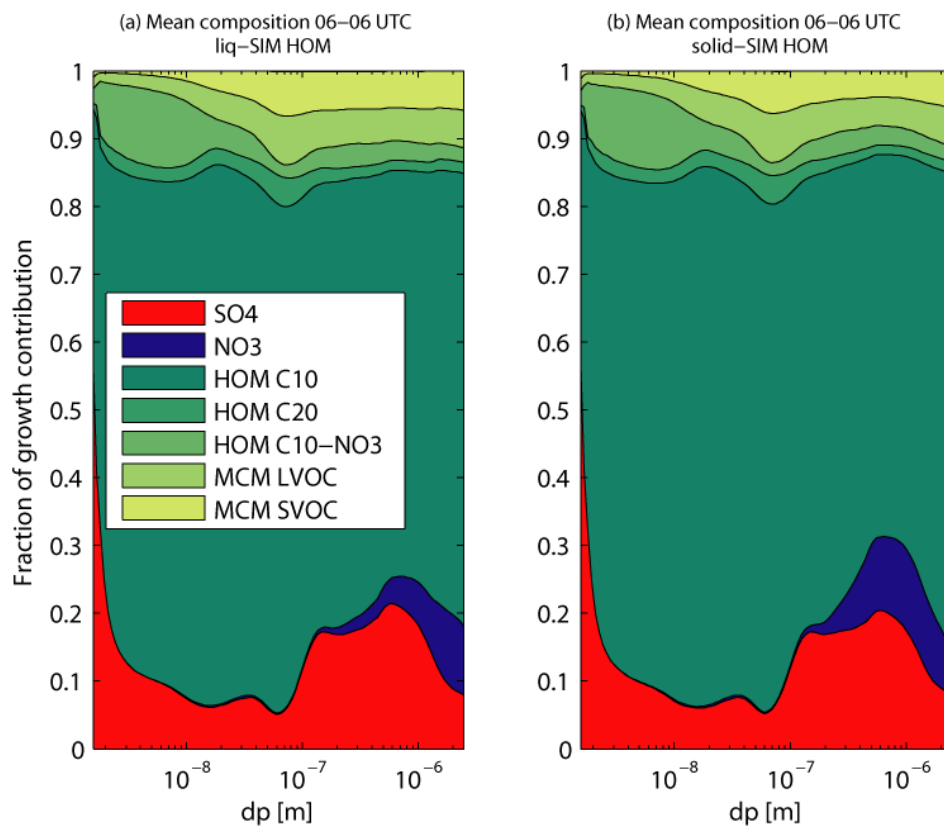


Figure S12. Mean mass fractions of the compound types that contribute to the growth of the particles during all chosen new particle formation events (from 06 UTC the morning of the event to 06 UTC the following day). In (a) the particles are assumed to be liquid with vapor pressures of HOMs estimated with SIMPOL. In (b) the particles are assumed to be solid with the same vapor pressure estimation.

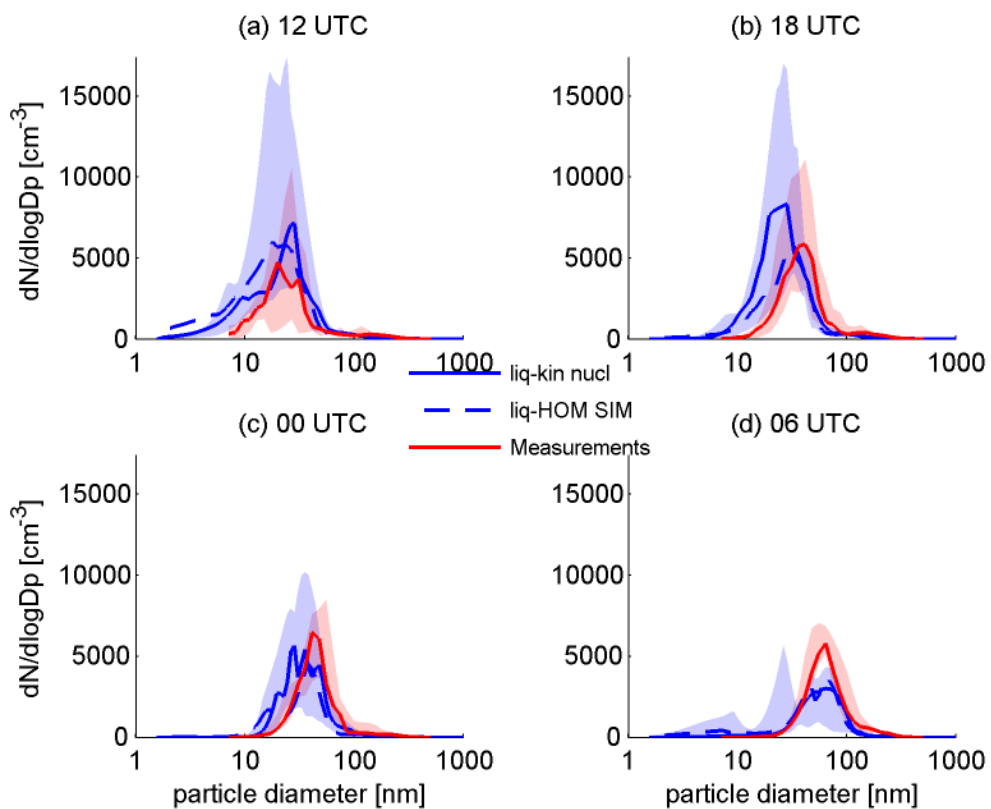


Figure S13. Measured (red lines), modeled with kinetic H₂SO₄ nucleation (solid blue lines) and modeled base-case scenario (dashed blue lines) median number size distributions at (a) 12 and (b) 18 UTC the day of the new particle formation event and (c) 00 and (d) 06 UTC the following day. The shaded areas are the values from the measurements and modeled liq-kin nucl that fall between the 25th and 75th percentiles.

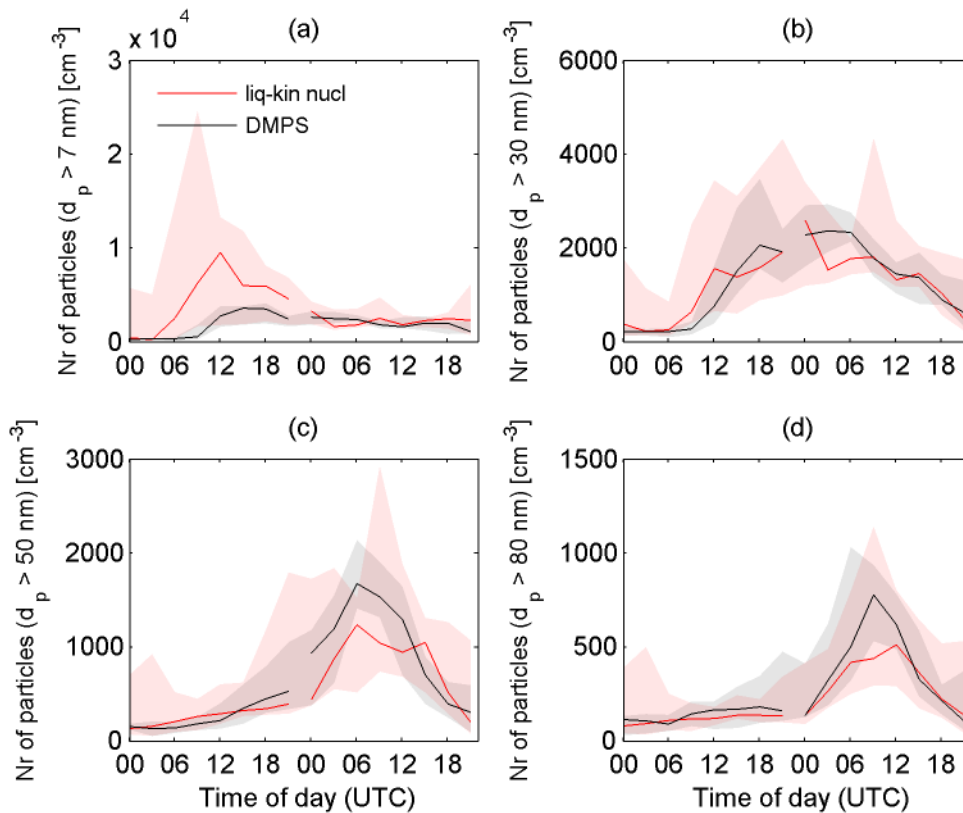


Figure S14. Median number of particles above (a) 7 nm, (b) 30 nm, (c) 50 nm and (d) 80nm of all chosen NPF-events at Pallas (from midnight at the day of the event to the evening the day after the start of the event) together with the 25 and 75 percentiles (shaded areas). The black lines are the median DMPS-data from Pallas and the red lines are the results from simulation liq-kin nucl where the nucleation rate was modeled with kinetic H_2SO_4 nucleation (Eq. 3).